Appl Phys A (2011) 104:1121–1128
DOI 10.1007/s00339-011-6387-z

Applied Physics A
Materials Science & Processing

Nanostructuring and hardening of LiF crystals irradiated with 3–15 MeV Au ions

J. Maniks · I. Manika · R. Grants · R. Zabels · K. Schwartz · M. Sorokin · R.M. Papaleo

Received: 15 July 2010 / Accepted: 15 March 2011 / Published online: 14 April 2011

Abstract Modifications of the structure and mechanical properties in LiF crystals irradiated with MeV-energy Au ions have been studied using nanoindentation, atomic force microscopy and optical spectroscopy. The nanostructuring of crystals under a high-fluence irradiation (above 10^{13} ions/cm^2) was observed. Nanoindentation tests show a strong ion-induced increase of hardness (up to 150–200%), which is related to the high volume concentration of complex color centers, defect aggregates, dislocation loops and grain boundaries acting as strong barriers for dislocations. From the depth profiling of the hardness and energy loss it follows that both nuclear and electronic stopping mechanisms of MeV Au ions contribute to the creation of damage and hardening. Whereas the electronic stopping is dominating in the near-surface region, the effect of elastic displacements prevails in deeper layers close to the projectile range.

J. Maniks (✉) · I. Manika · R. Grants · R. Zabels
Institute of Solid State Physics, University of Latvia, 8 Kengaraga Str., 1063 Riga, Latvia
e-mail: manik@latnet.lv
Fax: +371-671-32778

I. Manika
e-mail: manik@latnet.lv

R. Grants
e-mail: rolchix@gmail.com

R. Zabels
e-mail: rzabels@gmail.com

K. Schwartz
GSI Helmholtz Zentrum für Schwerionenforschung, Planckstr. 1, 64291 Darmstadt, Germany
e-mail: K.Schwartz@gsi.de

M. Sorokin
Russian Research Centre 'Kurchatov Institute', Moscow, Russia
e-mail: m40@lab2.ru

R.M. Papaleo
Faculty of Physics, PUCRS, Av. Ipiranga 6681, Porto Alegre, RS, Brazil
e-mail: papaleo@pucrs.br

1 Introduction

Beams of swift heavy ions with MeV–GeV energy have increasingly gained an interest for their application in a structural modification of materials and an improvement of their optical, electrical and other properties [1].

Peculiarities of a heavy-ion interaction with dielectrics are a fast energy deposition in a time scale shorter than the defect creation time, a high excitation density and a high gradient of absorbed energy in the ion track [2–5]. In LiF crystals heavy ions create fast electrons, which after a thermal relaxation induce electronic excitations of the lattice (excitons, electron–hole pairs). These lattice excitations after self trapping produce F–H Frenkel pairs (where the F center is an anion vacancy with a localized electron ($v_a{}^+e$) and the H center is an interstitial halogen molecule X_2^-). A higher dose (fluence) of the irradiation at room temperature leads to the transformation of primary F and H centers into more complex electron (F_2, F_3, F_4) and hole (V_3) centers (the V_3 center is a three-halide molecule $X_3^- = X^0X^-X^0$ in the lattice), halogen molecules ($H + H \rightarrow X_2$) and their clusters (nX_2) [2, 6].

An irradiation of LiF with ions in the MeV energy range shows some peculiarities relative to GeV ions. The MeV ions exhibit a comparable or higher elastic (nuclear) energy loss [6, 7]. Nevertheless, a more detailed analysis of the energy deposition of displaced atoms (recoils) shows that even for 3-MeV Au ions, where the elastic energy loss is twice the electronic one, the interaction of recoils with the crystal leads to a 66% fraction of the energy deposited into the

Table 1 Energy (E_{ion}) and charge (q) of incident Au ions, calculated inelastic (ionization) energy loss fraction (% of E_{ion}) and range (R) for Au ions of different energies in LiF

E_{ion}, MeV	Ion charge q	Inelastic losses, % of E_{ion}			Ion range R, μm
		Ions	Recoils	Total	
3	+2	30.9	35.5	66.4	0.67
5	+2	38.7	33.4	72.1	1.14
10	+4	49.9	29.2	79.1	2.29
12	+4	53.0	28.0	81.0	2.75
15	+6	58.5	24.4	82.9	3.49

electronic subsystem [8]. Having a projected range of a few micrometers, the MeV ions induce a volume concentration of color centers more than one order of magnitude higher than the GeV-energy ions with the same absorbed energy. The high volume concentration of primary Frenkel pairs, on the one hand, leads to a high electron–hole center recombination and, on the other hand, to more efficient coagulation processes leading to a formation of F_n centers as well as halogen molecules (X_2) and their aggregates [6]. These processes strongly depend on flux (beam current density) and fluence [9]. The coagulation of ion-induced defects produces strong modifications in the structure and properties of the target material. A high-fluence irradiation of LiF with swift heavy ions induces a pronounced increase of the indentation hardness which is sensitive to defect aggregates as strong obstacles for dislocations [10]. Indentation tests can provide information about defect aggregates on the surface as well as in the bulk of irradiated crystals.

In the presented study the modification of the structure and mechanical properties of LiF crystals irradiated with 3–15 MeV Au ions has been performed using optical absorption spectroscopy, nanoindentation, chemical etching and atomic force microscopy.

2 Experimental

Experiments were performed on nominally pure LiF single crystals grown from the melt in an inert atmosphere (Korth Kristalle, Germany). Main trace impurities were Mg and Na with the concentration of 20 ppm. The density of grown-in dislocations in the non-irradiated samples was about 5×10^4 cm^{-2}. Thin platelets were cleaved from a crystal block along the (100) planes. Crystals were irradiated at the Tandetron accelerator in Porto Alegre (Brazil) with 3-, 5-, 10- , 12- and 15-MeV Au ions at fluences of 10^{12}–2×10^{14} ions/cm^2 and ion beam current densities (i_{beam}) from 6.2 to 150 nA/cm^2. The flux (φ) can be estimated as $\varphi = 6.24 \times 10^9 \times i_{beam}/q$ ions cm^{-2} s^{-1}, where q is the charge of the ion (Table 1). In order to compare effects induced by MeV- and GeV-ion irradiations, LiF samples were irradiated at the UNILAC linear accelerator of the GSI, Darmstadt with 2.2-GeV Au ions at a fluence of 10^{12} ions/cm^2 with a flux of $\sim 10^8$ ions cm^{-2} s^{-1}. All irradiations were performed at room temperature and under normal incidence of the ions to the (100) cleavage face of the crystals. The irradiation parameters for LiF crystals and also the values of inelastic energy loss fraction (% of E_{ion}) and range (R) for Au ions which were calculated using the SRIM 2010 code [7] are presented in Table 1.

Optical spectroscopy was performed using a double-beam spectrometer (ATI Unicam UV4) in the spectral range of 190–700 nm. In this study only electron color centers (F, F_2, F_3, F_4) were tested, whereas the complementary V_3 centers have absorption in the vacuum UV spectral region (maximum at 114 nm) inaccessible with our equipment.

Nanoindentation tests were performed by a MTS G200 nanoindenter with a Berkovich diamond tip (curvature <20 nm) using the basic and continuous stiffness measurement techniques. Measurements were conducted at a load resolution <50 nN, a displacement resolution ≥1 nm, a strain rate of 0.05 s^{-1} and a harmonic frequency of 45 Hz. The nanoindenter was calibrated using a reference sample of fused silica. The hardness, Young's modulus and standard deviation of the measurements were calculated from experimentally obtained loading–unloading curves by the MTS TestWorks 4 software. Results were averaged from 10 individual measurements. Indentation tests were conducted on the irradiated surface in ambient air at room temperature. The depth profiles of hardness and modulus were obtained from the indentation tests on sample cross sections prepared by cleaving perpendicular to the irradiated surface. The distance of indents from the irradiated surface was measured by optical microscopy. The structural defects in irradiated crystals were revealed by chemical etching in a saturated aqueous $FeCl_3$ solution. The surface topography was studied with a Veeco CPII atomic force microscope in tapping mode using standard silicon probes with a tip radius of 10 nm.

3 Results

3.1 Color centers

The irradiation with 3–15 MeV Au ions in LiF produces Frenkel pairs (F–H) with a high volume concentration. This is illustrated in Fig. 1 for LiF irradiated with 15-MeV Au ions to a fluence of 5×10^{13} ions/cm^2 at two different flux (φ) values ($\varphi_1 = 6.5 \times 10^{10}$ and $\varphi_2 = 1.6 \times 10^{11}$ ions/cm^2 s). At the larger flux the number of created color centers is higher due to the enhanced formation of di-halide molecules

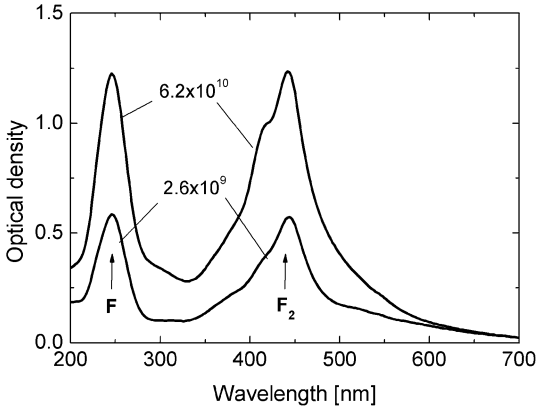

Fig. 1 Optical absorption spectra for LiF crystals irradiated with 15-MeV Au ions at fluence 5×10^{13} ions/cm^2. The ion beam flux values were 2.6×10^9 ions cm^{-2} s^{-1} and 6.2×10^{10} ions cm^{-2} s^{-1}

and their clusters, which prevents the recombination of mobile H centers with electron color centers [6].

The concentrations of F and F_2 centers can be estimated from the absorption spectra using the Smakula–Dexter formula [4]

$$n_F = 9.48 \times 10^{15} \times D_F \tag{1}$$

and

$$n_{F_2} = 4.42 \times 10^{15} \times D_{F_2}, \tag{2}$$

where D_F and D_{F_2} are the optical densities at the maximum of the absorption spectra for F (250 nm) and F_2 (445 nm) centers, respectively. According to (1), the number of created F centers for the higher flux (Fig. 1) is $n_F = 1.2 \times 10^{16}$ cm^{-2} with the volume concentration $N_F = n_F/R \sim 3.4 \times 10^{19}$ cm^{-3}. Such volume concentration is much higher than in crystals irradiated with GeV Au ions having the same absorbed energy [4, 5]. The high value of N_F stimulates the formation of F_n centers. We can estimate the concentration for F_n centers using the formula (2) with the approximation that the F_2 centers are dominating. The ratio $n_{F_2}/n_F = 0.47$, which is also remarkably higher than for GeV Au ions with the same absorbed energy (cf. [4], where $n_{F_2}/n_F = 0.2$). At a higher flux the efficiency of F center aggregation increases and higher concentrations of F_3 and F_4 centers are produced according to the reactions $F_2 + F \rightarrow F_3$ and $F_3 + F \rightarrow F_4$. The maxima of the absorption spectra of F_3 centers are at 317 and 377 nm and for F_4 centers at 518 and 540 nm, respectively. The increased concentrations of F_3 and F_4 centers lead to an extension of the absorption around the F_2 peak (Fig. 1).

Taking into account the high volume concentration of defect aggregates in crystals irradiated with 3–15 MeV Au ions, we can expect a stronger ion-induced effect on mechanical properties.

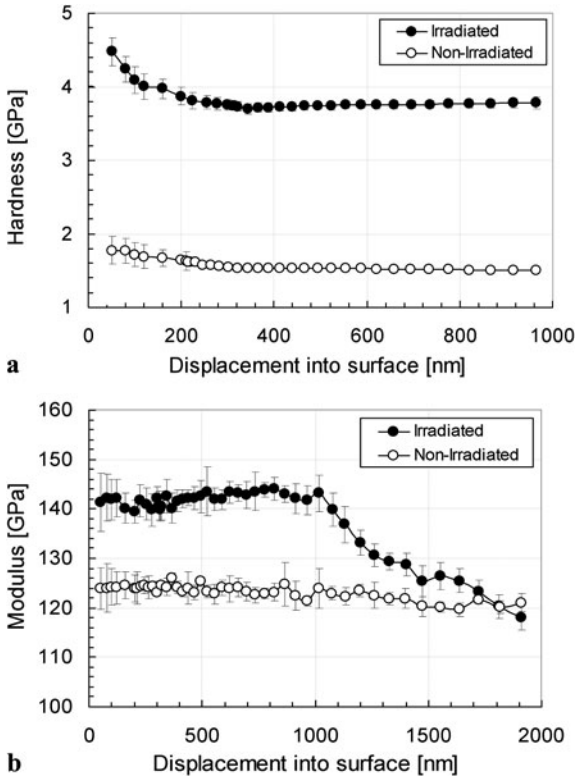

Fig. 2 Hardness (**a**) and Young's modulus (**b**) on the irradiated surface as a function of indentation depth for samples irradiated with 15-MeV Au ions at the fluence of 5×10^{13} ions/cm^2. The measured values for a non-irradiated LiF crystal are reported for comparison

3.2 Ion-induced changes of hardness and modulus

Nanoindentation tests showed a remarkable ion-induced increase of hardness which depends on the fluence and the ion energy. In order to exclude the effect of a softer bulk material, measurements were performed in a limited indentation depth range (≤ 0.3 of the thickness of the irradiated layer) in accordance with the recommendations for a given hardness ratio of irradiated and non-irradiated material [11].

Figure 2 demonstrates a typical result for the sample irradiated with 15-MeV Au ions. The hardness on the irradiated surface exceeds the hardness of a non-irradiated crystal by 150%, providing the evidence of a severe ion-induced damage and a formation of strong obstacles for dislocations. The ion-induced change of Young's modulus is comparatively small (about 15%, Fig. 2b) and lies in the typical range for stress-induced variations of modulus. Moreover, the sign of the effect changes from positive on the irradiated surface to negative in deeper layers, thus following the change of ion-induced stresses from compressive on the surface to tensile at the vicinity of the interface between irradiated and non-irradiated areas.

The dependence of hardness on fluence for all applied ion energies is shown in Fig. 3. The ion-induced hardening

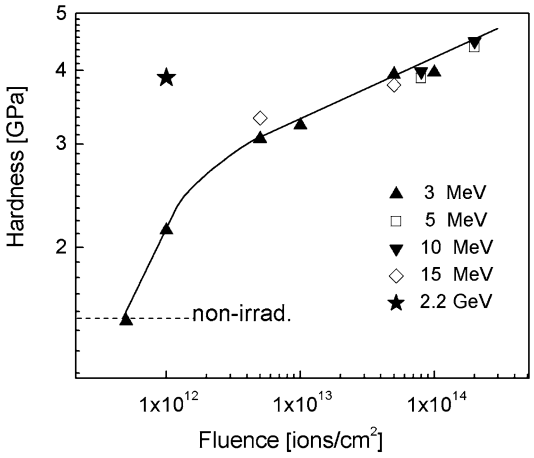

Fig. 3 Hardness as a function of fluence for LiF irradiated with 3-, 5-, 10- and 15-MeV Au ions. The irradiation is performed at an ion beam current density of 100 nA/cm^2. The measured value for the irradiation with 2.2-GeV Au ions is also reported

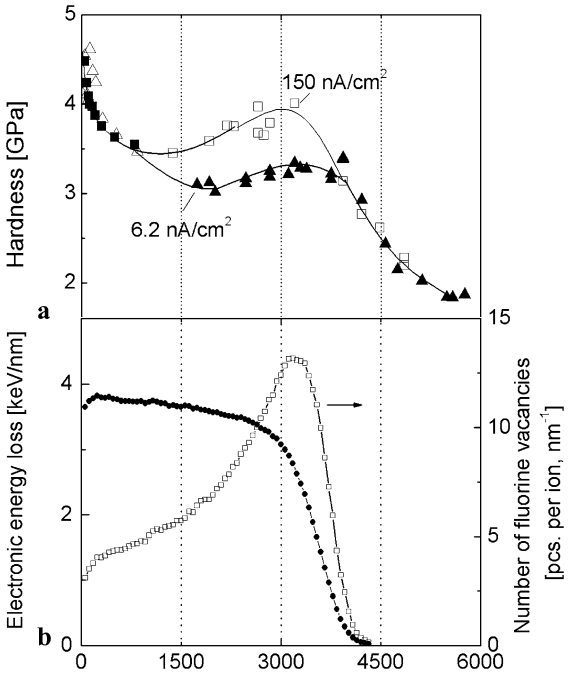

Fig. 4 (**a**) The depth profile of hardness of LiF irradiated with 15-MeV Au ions; the density of ion beam current was 6.2 and 150 nA/cm^2; (**b**) the calculated depth profiles of electronic energy loss (*circles*, *left-hand axis*) and fluorine vacancies, created by elastic displacements (*open squares*, *right-hand axis*)

is observed at fluences above the threshold of 10^{12} ions/cm^2. The hardness increases with the fluence and saturates at the fluence of 10^{14} ions/cm^2. The saturation value of hardness (∼4.5 GPa) exceeds by a factor of three the hardness of a virgin crystal. The hardness data for all applied ion energies settle on a common curve, thus indicating that the ion-induced hardening is nearly independent of energy. Obviously, such behavior emerges from the fact that the local deposited energy (E/R) in the investigated range of ion energies is almost constant (see Table 1). However, an increase of the energy leads to an increase of the depth of the hardened layer in accordance with the change of the ion range.

Depth profiles of the hardness were measured on the cross section of irradiated crystals. A detailed study was performed on samples irradiated with 15-MeV Au ions with the flux of 2.6 and 6.2 ions cm^{-2} s^{-1}. To access the near-surface region, results are supplemented with the hardness–indentation depth data from measurements on the irradiated surface. Hardness as a function of the distance from the irradiated surface is plotted in Fig. 4a. The hardness curve displays two maxima: (1) on the irradiated surface and (2) close to the end of the ion pass. A stronger hardening on the surface is typical for irradiations with swift heavy ions [10]. The hardening maximum in bulk is sensitive to the ion beam current density and increases with the current. The hardened zone is slightly extended beyond the projectile range. In order to compare the nanoindentation data with the fraction of the energy actually absorbed by the target material, we used the SRIM code in the mode of a detailed calculation with full damage cascades as described in [8]. It was taken into account that the primary knocked target atoms have the energy high enough to deposit a considerable fraction of the energy in inelastic collisions inside the material. The calculated data of the electronic energy loss contributed both by projectile ions and recoils and the calculated profile of fluorine vacancies created by elastic displacements for 15-MeV Au ions are plotted in Fig. 4b. From the comparison of depth profiles of the hardness and the energy loss, it follows that both nuclear and electronic stopping mechanisms of MeV Au ions contribute to the creation of damage and hardening. Whereas the electronic stopping is dominating in the near-surface region, the effect of elastic displacements prevails in deeper layers close to the projectile range.

To compare effects produced by MeV and GeV ions, the nanoindentation tests were performed also on LiF samples irradiated with 2.2-GeV Au ions at the fluence of 10^{12} ions/cm^2, at which ion tracks strongly overlap and the effect of the ion-induced hardening saturates. An observed increase in the hardness in the case of the GeV-ion irradiation reaches up to 3.9 GPa, which is in accordance to the previous research results [10]. To achieve the same hardening by MeV ions a higher fluence is required (see Fig. 3) but the absorbed energy in comparison to GeV ions is lower. The irradiation at an ion beam current density of 100 nA/cm^2 corresponds to the flux of 3.12×10^{11} ions cm^{-2} s^{-1} for 3- and 5-MeV, 1.56×10^{11} ions cm^{-2} s^{-1} for 10-MeV and 10^{11} ions cm^{-2} s^{-1} for 15-MeV Au ions. The flux for 2.2-GeV Au ions was $\varphi \approx 10^8$ ions cm^{-2} s^{-1}. The absorbed ion energy $E_{\text{ion}} \times \Phi$ for 2.2-GeV Au ions ($\Phi = 10^{12}$ ions/cm^2) is 2.2×10^{21} eV/cm^2 and for 3-MeV Au ions ($\Phi = 10^{14}$ ions/cm^2) is 3×10^{20} eV/cm^2.

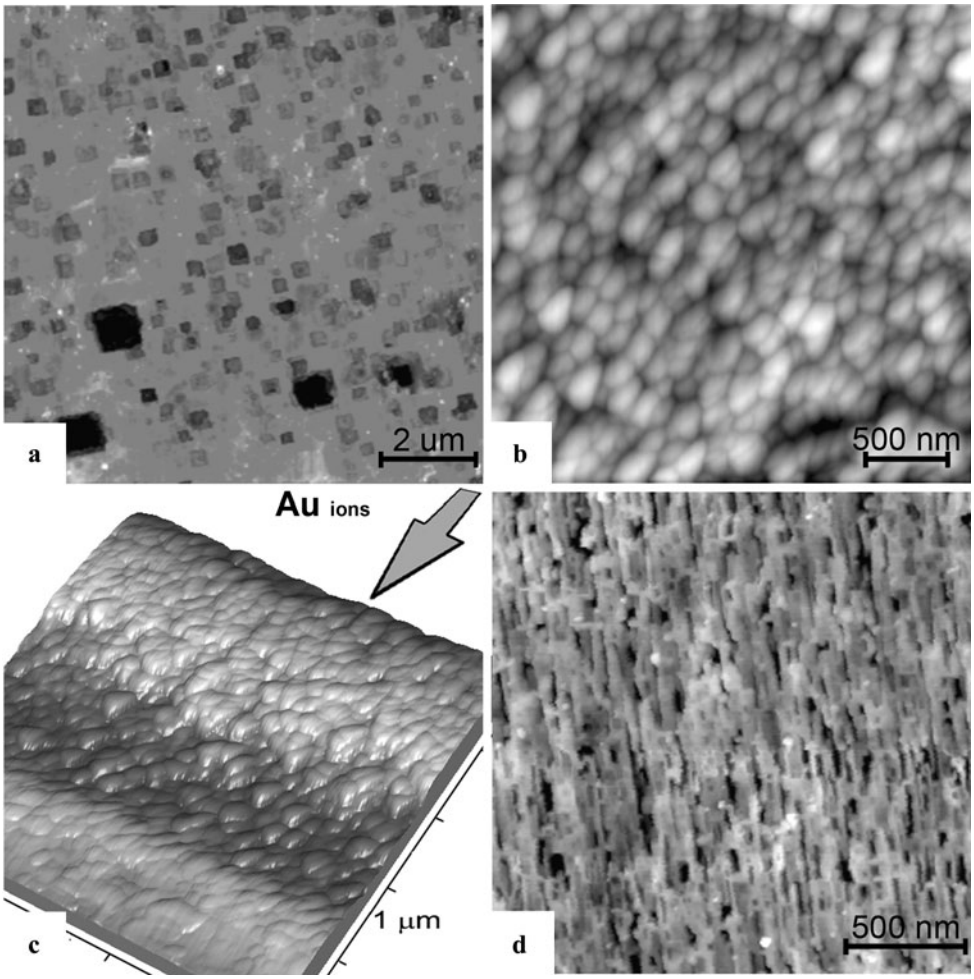

Fig. 5 AFM images of the irradiated surface: (**a**) after irradiation with 3-MeV Au ions at $\Phi = 10^{12}$ ions/cm^2 and (**b**) after irradiation with 15-MeV Au ions at $\Phi = 5 \times 10^{13}$ ions/cm^2; AFM images of the sample's cross section: (**c**) after irradiation with 15-MeV Au ions at $\Phi = 5 \times 10^{13}$ ions/cm^2 and (**d**) after irradiation with 2.2-GeV Au ions at $\Phi = 10^{12}$ ions/cm^2

3.3 Ion-induced modifications of structure

Investigations of the structure were performed on the irradiated surface and on the cross section of samples prepared by cleaving perpendicular to the irradiated surface. Detailed studies were performed on samples irradiated with 3- and 15-MeV Au ions. In order to reveal structural defects, samples were treated by a chemical etching. The results of the optical and atomic force microscopy (AFM) study showed that the density of dislocations in non-irradiated crystals varies in the range of 5×10^4 to 10^6 cm^{-2} depending on a cleavage procedure. After an irradiation at fluences up to 5×10^{12} ions/cm^2, a large amount of new dislocations was revealed (Fig. 5a). Their density increased with the fluence and reached about 10^9 cm^{-2}. Etch pits of ion-induced dislocations were smaller compared to those for pre-existing dislocations. In many cases etch pits were flat bottomed, as is typical for prismatic dislocations of vacancy and interstitial types. The identical orientation of dislocation etch pits gives the evidence for a maintained single-crystalline structure of the irradiated samples.

After the irradiation at the fluence 10^{13} ions/cm^2 first indications a nanostructuring were observed. At the fluence 5×10^{13} ions/cm^2 the irradiated layer became uniformly nanostructured. AFM images of the irradiated surface show a structure consisting of clusters with the size of 50–150 nm (Fig. 5b). The three-dimensional image of the sample's cross section shows the irradiated layer consisting of columnar grains (Fig. 5c). The thickness of the nanostructured layer (∼3.5 μm) coincides with the calculated range of 15-MeV Au ions in LiF. The formation of a nanostructure in LiF samples was also observed under the irradiation with 2.2-GeV-energy Au ions. The irradiated layer consists of long columnar grains with a cross section of about 50–100 nm (Fig. 5d). Its structure on the irradiated surface is similar to that shown in Fig. 5b.

The thermal stability of nanostructures was assessed by annealing irradiated samples at 750 K for 10 min. A recovery of the structure and the hardness after the annealing was observed. An exception was the samples irradiated at the highest current density (150 nA/cm^2) for which a small residual effect of hardening and an increased density of dislocations was observed.

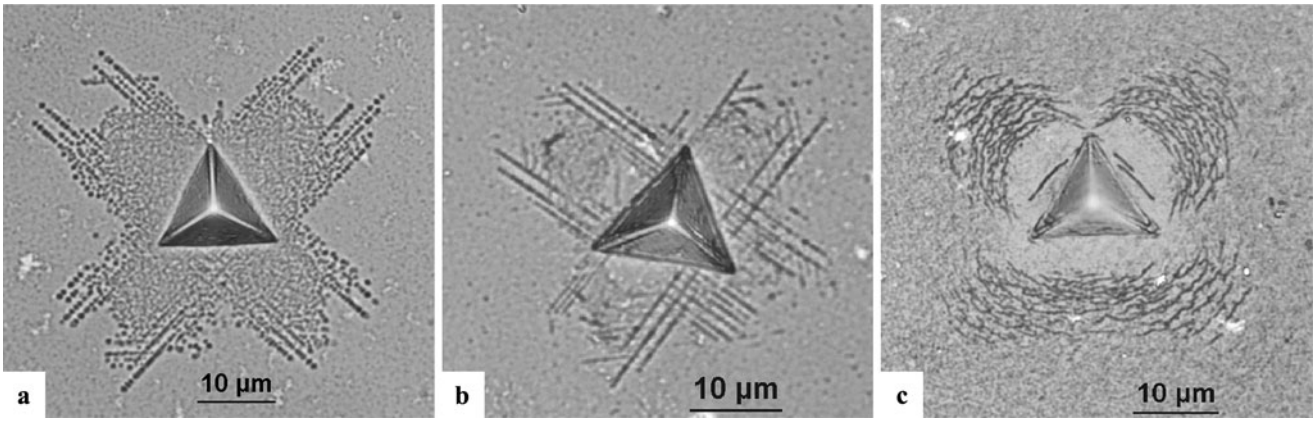

Fig. 6 Optical images of the deformation zone around indents (after chemical etching): (**a**) on the virgin surface, (**b**) and (**c**) on surfaces irradiated with 3-MeV Au ions at the fluences of 10^{12} and 5×10^{13} ions/cm^2, respectively

Figure 6 shows the evolution of the deformation zone at the indentation test. In non-irradiated samples a typical dislocation rosette is formed, confirming the dislocation gliding on {110} planes along the ⟨110⟩ axis. After an irradiation at moderate fluences, a dislocation rosette shows indications of a dislocation hindering. In samples, which were nanostructured under the high-fluence irradiation, no preferable directions of the deformation were observed, and the deformation mode was similar to that for isotropic solids where the maximum of stress and deformation is produced against the centers of indenter faces (Fig. 6c). A crack pattern around the indent is formed, indicating immobilization of dislocations by radiation defects.

4 Discussion

The optical absorption spectra for LiF irradiated with Au ions of MeV energy show the formation of a broad spectrum of damage products, such as single F centers, F_2, F_3, F_4, as well as F_3^+ etc. The concentration of produced F_n centers and defect aggregates achieved by an irradiation with 3–15 MeV ions is higher than that for GeV Au ions [6, 8, 9]. The structural study reveals additional defects, such as dislocations and grain boundaries.

A strong ion-induced increase of the indentation hardness as a structure-sensitive characteristic is observed. The deformation at the indentation test occurs under a high local stress and the produced dislocations are moving at a high velocity (up to 10^5 cm/s [12]) that allows surmounting point defects, single color centers and other comparatively weak obstacles. As a result, single defects play a minor role in the ion-induced hardening. However, weak obstacles can reduce the mobility of dislocations moving at low velocity, as follows from measurements of the arm length of a dislocation pattern around indents [10, 13]. The nanohardness is sensitive mainly to dislocations, closely spaced aggregates of radiation defects and grain boundaries. According to the additivity rule, the resulting hardening is a superposition of different strengthening phenomena.

Discrete obstacles, particularly in the form of precipitates, aggregates of point defects of various types and even nanoscale cavities can alter the hardness by the dispersion strengthening mechanism. According to Orowan's model, the stress (σ) required for a dislocation to pass an array of particles spaced at the distance λ is given by

$$\sigma = \sigma_0 + \frac{\alpha G b}{\lambda}, \tag{3}$$

where σ_0 is the yield strength of the non-irradiated crystal, G is the shear modulus, b denotes the Burgers vector and α characterizes the obstacle strength [14]. An identical relation holds for the indentation hardness. Brief estimates performed by (3) using the hardness of the matrix $H_0 = 1.5$ GPa, $G = 45.8$ GPa, $b = 2.84 \times 10^{-10}$ m and $\alpha = 1$ show that a detectable increase of the hardness is expected at the average obstacle spacing $\lambda < 200$ nm. Such conditions are fulfilled at high-fluence irradiations at the stage of track overlapping.

The strength properties of crystalline solids strongly depend on the density of dislocations. It is well established that dislocation loops of vacancy and interstitial types are formed in alkali-halide crystals by different kinds of high-dose irradiation under conditions of saturation and an aggregation of single defects [15, 16]. Another source of dislocations are the ion-induced elastic stresses, which in irradiated samples can reach a critical value [17]. Accumulation of dislocations under a high-fluence irradiation leads to a formation of dislocation networks and their transformation to grain boundaries. Such evolution of the structure ensures a reduction of ion-induced elastic stresses. Ion-induced dislocations cause an increase of the flow stress and the hardness. The flow

stress (τ) is related to the density of dislocations (ρ) through Tailor's relationship

$$\tau = \tau_m + \beta G b \sqrt{\rho}, \quad (4)$$

where G is the shear modulus of the matrix and τ_m is its flow stress; β is a constant, which varies in the range of 0.05–1.5 [14]. Estimates by (4) show that strength properties markedly increase at dislocation densities above 10^7 cm^{-2}. This limit of the created dislocation density is surpassed in irradiation experiments presented here.

The nanostructuring of LiF under the irradiation creates a large volume fraction of boundaries. Grain boundaries serve as obstacles for dislocations and have a significant impact on mechanical properties, e.g. yield strength and hardness. For many materials the yield strength (σ) is related to a grain size (d) through the Hall–Petch equation

$$\sigma = \sigma_0 + k d^{-1/2}, \quad (5)$$

where σ_0 and k are constants [18, 19].

As shown in Fig. 3, the hardness of the nanostructured LiF saturates at about 4.5 GPa. Obviously, further increase of the hardness is limited due to the initiation of a brittle fracture in the indentation zone as shown in Fig. 6c. However, a remarkable hardening is observed before the stage of a uniform nanostructuring that confirms a considerable strengthening by dislocations, colloids and other aggregates of point defects.

The dislocations and grain boundaries serve as sinks for mobile radiation defects and seeds for a nucleation and a growth of defect aggregates, thus affecting the aggregation and annihilation processes of single defects. Besides, the segregation of defects on dislocations and grain boundaries reduces their mobility and facilitates the ion-induced hardening.

The irradiation effects are largely controlled by the energy absorbed in the target material and by concentrations of point defects which are introduced during displacement cascades. A comparison between depth profiles of hardness and energy loss is given in Fig. 4. A stronger hardening on the irradiated surface can be related to a higher electronic energy loss at a vicinity to the surface and partially also to specific surface processes. The collision of high-energy ions with the crystal surface causes a variety of phenomena, such as a sputtering of target atoms and a segregation of mobile radiation defects on the surface. The above-mentioned processes can lead to the compositional and structural change. Additional modifications could be caused during the post-irradiation stage by the environmental attack. The second maximum of hardness is observed in the bulk of the irradiated layer close to the end of the ion path, where a production of vacancies and interstitials in displacement cascades displays a maximum and an aggregation of single defects is facilitated. As shown in Fig. 4a, this maximum increases with the ion beam current. Such effect can be explained by the noticeable rise of the creation efficiency for the aggregates of F centers and intrinsic lithium colloids under conditions when a high fluence is accumulated with a high flux of ions [8, 9]. At high flux and fluence the concentration of H centers is high and the interaction between them takes place. Such interaction leads to a formation of hole centers, di-halide molecules and fluorine bubbles and reduces the number of free H centers which are able to recombine with F centers. As a result, the concentration of F centers increases and their aggregation is facilitated.

Structural modifications of LiF are of a special interest. In contrast to many insulators, LiF does not amorphize even under a high dose of irradiation. This property is characteristic for materials with a strong ionic bonding. An irradiation with swift ions typically leads to the formation of a composite-like structure in which the crystalline LiF matrix is interwoven with linear ion tracks and embedded with nanometer-sized defect aggregates. Studies of the nanostructuring are concerned mainly with modifications of the surface topography, including an ion-induced formation of hillock- or crater-type nanostructures and figures of ion sputtering [20, 21]. Fragmentation processes, which lead to the reduction of the grain size, are observed in polycrystalline LiF films under the irradiation with MeV-energy Au ions [22]. The present study shows that the high-fluence irradiation of LiF single crystals with MeV–GeV Au ions leads to the formation of the bulk nanostructure consisting of grains with nanoscale dimensions.

5 Conclusion

The ratio of concentrations of complex F_n to single F centers in LiF crystals irradiated with 3–15 MeV Au ions is higher than in case of GeV Au ions with a similar absorbed energy. This explains higher changes in mechanical properties under the MeV-ion irradiation. The strong hardening (up to 150–200%) of LiF crystals under the irradiation with MeV-energy Au ions is observed. Structural studies reveal the formation of dislocations and nanostructuring under the high-fluence irradiation. The ion-induced hardening is related to dislocation impeding by assemblies of defect aggregates, such as dislocation loops of vacancy and interstitial types, grain boundaries, molecular fluorine clusters, lithium colloids etc.

Both nuclear and electronic stopping mechanisms of MeV Au ions in LiF contribute to the damage creation and hardening. Whereas the electronic stopping is dominating in the near-surface region, the effect of elastic displacements prevails in deeper layers, close to the projectile range.

Acknowledgements This research was partly supported by the Latvian Government grant no. 09.1548 M. Sorokin greatly acknowledges support from the Russian Foundation for Basic Research (grant nos. 08-08-00603 and 09-08-12196).

References

1. M. Toulemonde, C. Trautmann, E. Balanzat, K. Hjort, A. Weidlinger, Nucl. Instrum. Methods B **256**, 346 (2007)
2. N. Itoh, A.M. Stoneham, *Materials Modification by Electronic Excitations* (Cambridge University Press, Cambridge, 2001)
3. N. Itoh, D.M. Duffy, S. Khakshouri, A.M. Stoneham, J. Phys., Condens. Matter **21**, 474205 (2009)
4. K. Schwartz, A.E. Volkov, M.V. Sorokin, C. Trautmann, K.-O. Voss, R. Neumann, M. Lang, Phys. Rev. B **78**, 0241120 (2008)
5. C. Trautmann, K. Schwartz, J.M. Costantini, T. Steckenreiter, M. Tolulemonde, Nucl. Instrum. Methods B **146**, 367 (1998)
6. K. Schwartz, M.V. Sorokin, A. Lushchik, Ch. Lushchik, E. Vasil´chenko, R.M. Papaleo, D. de Souza, A.E. Volkov, K.-O. Voss, R. Neumann, C. Trautmann, Nucl. Instrum. Methods B **266**, 2736 (2008)
7. J.F. Ziegler, P. Biersack, U. Littmark, *The Stopping and Range of Ions in Matter* (Pergamon, New York, 1985). SRIM—version 2010.01
8. M.V. Sorokin, R.M. Papaleo, K. Schwartz, Appl. Phys. A **97**, 143 (2009)
9. A. Lushchik, Ch. Lushchik, K. Schwartz, E. Vasil´chenko, R. Papaleo, M. Sorokin, A.E. Volkov, R. Neumann, C. Trautmann, Phys. Rev. B **76**, 054114 (2007)
10. I. Manika, J. Maniks, K. Schwartz, J. Phys. D, Appl. Phys. **41**, 074008 (2008)
11. I. Manika, J. Maniks, Thin Solid Films **144**, 257 (1992)
12. W.G. Johnston, J.J. Gilman, J. Appl. Phys. **30**, 129 (1959)
13. A.A. Urusovskaya, G.G. Knab, Phys. Status Solidi A **80**, 59 (1975)
14. F.R.N. Nabarro, M.S. Duesbery (eds.), *Dislocations in Solids*, vol. 10 (Elsevier, Amsterdam, 1996)
15. Y. Kawamata, J. Phys. **12**, C502 (1976)
16. L.W. Hobbs, J. Phys. **34**, C9-227 (1973)
17. I. Manika, J. Maniks, K. Schwartz, M. Toulemonde, C. Trautmann, Nucl. Instrum. Methods B **209**, 93 (2003)
18. E.O. Hall, Proc. Phys. Soc. Ser. B **64**, 747 (1951)
19. H. Gleiter, B. Chalmers, *High-Angle Grain Boundaries* (Oxford, Pergamon, 1972)
20. A. Müller, R. Neumann, K. Schwartz, C. Trautmann, Nucl. Instrum. Methods B **146**, 393 (1998)
21. V. Mussi, F. Granone, T. Marolo, R.M. Montereali, C. Boragno, F. Buatier de Mongeot, U. Valbusa, Appl. Phys. Lett. **88**, 103116 (2006)
22. M. Kumar, F. Singh, S.A. Khan, A. Tripathi, D.K. Avasthi, A.C. Pandey, J. Phys. D, Appl. Phys. **39**, 2935 (2006)